

6-16-2018

## Infrasound Tornillos Produced by Volcán Cotopaxi's Deep Crater

J. B. Johnson  
*Boise State University*

M. C. Ruiz  
*Escuela Politecnica Nacional*

H. D. Ortiz  
*Pontificia Universidad Católica del Ecuador*

L. M. Watson  
*Stanford University*

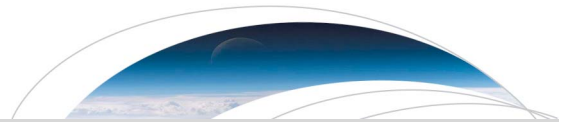
G. Viracucha  
*Escuela Politecnica Nacional*

*See next page for additional authors*

---

**Authors**

J. B. Johnson, M. C. Ruiz, H. D. Ortiz, L. M. Watson, G. Viracucha, P. Ramon, and M. Almeida



# Geophysical Research Letters

## RESEARCH LETTER

10.1029/2018GL077766

### Key Points:

- An infrasonic tornillo, a very low-frequency, low damped signal, is identified at Cotopaxi Volcano
- The tornillo corresponds to resonance and reverberation within the crater and may be used to infer crater dimension and sound speeds
- Apparent negative polarity “first motions” may be related to modulating influences of the crater’s extreme topography

### Supporting Information:

- Supporting Information S1

### Correspondence to:

J. B. Johnson,  
jeffrejbjohnson@boisestate.edu

### Citation:




Johnson, J. B., Ruiz, M. C., Ortiz, H. D., Watson, L. M., Viracucha, G., Ramon, P., & Almeida, M. (2018). Infrasonic tornillos produced by Volcán Cotopaxi’s deep crater. *Geophysical Research Letters*, 45, 5436–5444. <https://doi.org/10.1029/2018GL077766>

Received 5 MAR 2018

Accepted 7 MAY 2018

Published online 13 JUN 2018

## Infrasonic Tornillos Produced by Volcán Cotopaxi’s Deep Crater

J. B. Johnson<sup>1</sup> , M. C. Ruiz<sup>2</sup> , H. D. Ortiz<sup>3</sup>, L. M. Watson<sup>4</sup> , G. Viracucha<sup>2</sup>, P. Ramon<sup>2</sup>, and M. Almeida<sup>2</sup>

<sup>1</sup>Department of Geosciences, Boise State University, Boise, ID, USA, <sup>2</sup>Instituto Geofísico, Escuela Politécnica Nacional, Quito, Ecuador, <sup>3</sup>Escuela de Ciencias Físicas y Matemática, Pontificia Universidad Católica del Ecuador, Quito, Ecuador, <sup>4</sup>Department of Geophysics, Stanford University, Stanford, CA, USA

**Abstract** We characterize and interpret a new type of infrasonic signal originating from the summit of Volcán Cotopaxi (Ecuador) that was primarily observed between September 2015 and March 2016, following the 2015 eruptive period. This infrasonic waveform is a slowly decaying sinusoid with exceptional low-frequency ( $f_p = 0.2$  Hz) and high quality factor ( $Q = \sim 10$ ) and resembles the shape of tornillo seismic waveforms. The repeating events, occurring about once per day in early 2016, are stable in frequency content, and we attribute them to excitation of a vertical-walled crater, with radius of about 125 m and length of 300 m. Spectral properties of the tornillo permit constraints on crater sound speed ( $335 \text{ m/s} \pm 6\%$ ) and temperature ( $4\text{--}32^\circ\text{C}$ ). The initial polarity of the tornillos is predominantly a rarefaction and could reflect repeating crater bottom collapse events (implosions) or explosion sources whose infrasonic is heavily modulated by the crater’s pipe-like geometry.

**Plain Language Summary** Active volcanoes produce intense infrasonic, or low-frequency sounds below 20 Hz, which may be recorded with specialized microphones many kilometers from a volcanic crater. An objective of volcano infrasonic research is to infer volcano source processes, such as explosions, and the modulating influences of topographic effects and atmospheric transmission. This study reports on a novel type of signal recorded at Cotopaxi Volcano (in Ecuador) where the infrasonic possesses a remarkably low frequency and reverberates for many tens of seconds. We attribute the form of these infrasonic events to the geometry of Cotopaxi’s crater, which is a deep, steep-walled cylinder about 300-m deep and with a diameter of approximately 125 m and acts like a gigantic pipe resonator.

### 1. Introduction

*Tornillos*, or screw-shaped seismograms, refer to low-frequency earthquakes that were documented at Galeras Volcano (Colombia) in the early 1990s (Gómez & Torres, 1997; Narváez et al., 1997) and reported at many additional volcanoes, including Asama (Japan; Shimosuzu & Kagiyama, 1989), Kelut (Indonesia; Lesage & Surono, 1995), Tongariro (New Zealand; Hagerty & Benites, 2003), and Mount Griggs in Alaska (De Angelis, 2006). Common properties of the seismic tornillo include monochromatic frequency content and high quality factors, which contribute to a slowly decaying sinusoid signal that may endure for several tens of seconds. Tornillo generation in the aforementioned studies has been attributed to resonance of fluid-filled cavities, and their properties may be related to cavity size and sound speeds in the resonating fluid composed of ash and gas (Konstantinou, 2015).

Tornillo-shaped infrasonic recordings, unlike seismic tornillos, have not been prominently featured or well described in the literature, although there are some examples that have been presented in previous work (e.g., Spina et al., 2014, Figure 11). More commonly, monochromatic infrasonic pulses with narrow-peaked frequency spectra (i.e., high quality factors) have been reported at a range of open-vent volcanic systems, for example, Kilauea (Hawaii; Fee et al., 2010), Villarrica (Chile; Goto & Johnson, 2011), Etna (Italy; Spina et al., 2014), Erebus (Antarctica; Rowe et al., 2000), and Pagan (Mariana Islands; Lyons et al., 2016). Such signals are typically associated with explosions composed of an initial compression followed by only a few, quickly attenuated oscillations. The Cotopaxi infrasonic signals highlighted here stand out because they begin abruptly, often with an initial negative or ambiguous polarity, and continue with an extraordinary low fundamental frequency ( $\sim 0.2$  Hz) and with high- $Q$  coda oscillations lasting more than a minute. This study characterizes these repeating “infrasonic tornillos” and speculates on their source genesis, which we contend is heavily modulated by Cotopaxi’s extreme crater geometry.

## 2. Cotopaxi and Its Recent Eruptive History

Cotopaxi is a hazardous glacier-clad stratovolcano situated in Ecuador's Cordillera Central approximately 60 km southeast of the capital city Quito. The 5,987-m-tall edifice possesses a single symmetric summit crater, which sourced the eruptions of 2015. These eruptions were the first in more than 70 years and peaked during the late summer and fall of 2015 (Troncoso et al., 2017). During the eruption crisis magma appears to have intruded relatively shallow portions of the volcano, erupting juvenile ash, and progressively drying out the hydrothermal system (Gaunt et al., 2016).

Cotopaxi's 2015 eruptions and their precursors were well monitored by the Instituto Geofísico of the Escuela Politécnica Nacional (IGEPN in Quito) using seismic, geodetic, infrasound, visual, and gas remote sensing instrumentation. An increase in earthquake counts, deformation, and sulfur emissions was noted as early as April, 4 months prior to 14 August, when two large phreatic explosions occurred and "opened the system" (Bernard et al., 2016; Gaunt et al., 2016; Troncoso et al., 2017). These explosions occurred in quick succession and generated an eruption column that rose to an estimated height of nearly 9 km and was reported by the Washington Volcanic Ash Advisory Center. Total ash erupted was on the order of  $10^9$  kg and was reported as VEI 2 (Bernard et al., 2016). Following the August eruptive activity ash and steam emissions continued intermittently and were related to both real-time seismic amplitude measurements (RSAM) and fluctuations in daily earthquake counts. Eruptive activity progressively diminished in intensity until the last significant ash emission, which occurred on 18 November 2015. After this, smaller gas and ash emissions continued in 2016 and were identified using the seismic network and IGEPN telemetered cameras when summit visibility was good.

## 3. Infrasound Monitoring at Cotopaxi

Telemetered infrasound was recorded at Cotopaxi throughout the crisis from the five-station Japan International Cooperation Agency (JICA) network distributed around the volcano at distances of 2 to 6 km (Figure 1). The first clearly identified infrasound *tornillo* occurred on 1 September 2015, more than 2 weeks after the large explosions on 14 August. Prior to this period *tornillos* had not been recorded during approximately 10 years of infrasound monitoring; however, between September and December 2015 at least 37 infrasound *tornillos* were identified, of which ~12 were picked on multiple JICA stations. *Tornillo* events occurring during periods of clear weather comprise a small subset of the catalog, but they all seem to coincide with visible emission of gas and sometimes ash. Infrasound *tornillos* are also correlated with seismic events thought to be "buried explosion earthquakes" that have been located high up in the volcanic edifice and possibly at the bottom of the summit crater.

We installed a telemetered infrasound array CIS in December of 2015 in order to improve detection capabilities of potential low-vigor vent activity, including small explosions, gas exhalations, and *tornillos*. CIS consisted of a six-element, ~50-m aperture array located 8.3 km to the northwest of the active summit crater (Figures 1c and 1d). Although this array was installed farther from the vent than the stations of the JICA network, it was situated in a vegetated, low-noise environment and adjacent to existing IGEPN infrastructure with real-time telemetry capabilities. The infrasound sensors comprising the CIS array were microelectromechanical systems-based transducers with a flat frequency response above ~0.05 Hz (20 s) similar to those described by Marcillo et al. (2012).

The CIS infrasound array was installed at Cotopaxi after the primary (explosive) period in the fall of 2015 and at a time when overflights revealed a large vertical-walled summit crater (>100 radius) with uncertain depth because the bottom was generally obscured by vapor (Figure 1b). On 30 January 2018 an overflight with a thermal camera was used to determine that the open conduit extended more than 122 m below the inner crater rim. Given the oblique imagery (Figure 1b inset), the crater bottom was out of sight and probably much deeper. Cotopaxi's pipe-like crater morphology, copious degassing, and infrasound signals suggest that it was an open vent system during 2015 and 2016. An infrasound record from a JICA station on 18 November 2015, for instance, indicates 11 hr of continuous infrasound concentrated at about 0.2 Hz. Such infrasound tremor is similar to, but of substantially lower frequency than, the infrasound tremor commonly recorded at open-vent volcanoes such as Villarrica (Goto & Johnson, 2011) or Kilauea (Fee et al., 2010). Cotopaxi tremor episodes, however, were fairly uncommon and are not further discussed in this paper.

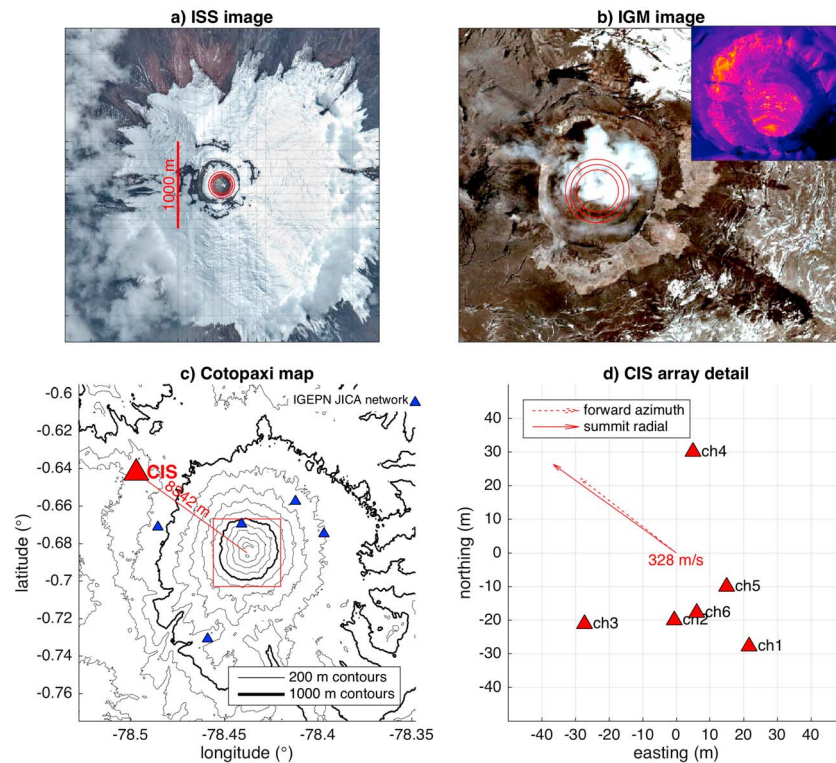


**Figure 1.** Cotopaxi maps and station locations. (a) International Space Station (ISS) image showing preeruption summit crater and glacier. (b) Orthophoto detail of summit produced by the Instituto Geografico Militar de Ecuador (IGM) from 28 January 2016. The red circles in panels (a) and (b) show 100-, 125-, and 150-m radii and correspond to a range of potential inner crater dimensions. Inset image in (b) shows oblique thermal image from 30 January 2018 with clear view of the top part of the vertical inner shaft. Maximum brightness temperatures are less than 100°C. (c) Topographic map, constructed from Shuttle Radar Topography Mission data, indicates location of infrasound array CIS, the Japan International Cooperation Agency (JICA) network, and the ISS image extent (red box). (d) Detail of the CIS array shows vent radial direction and inferred forward azimuth of tornillo signal.

The majority of Cotopaxi infrasound detections consisted of sporadic (~1 per day) extremely low-frequency (~0.2 Hz) transients that we refer to as infrasound tornillos.

#### 4. Detection of Infrasound Tornillos

The CIS array permitted definitive identification of the summit crater as the source of these tornillos. Phase delays between infrasound arriving on channels 1 and channels 2 through 6 were determined using signal cross correlation (Figure 2b), and comparison of these phases lags was made with delays computed for a range of candidate slowness vectors ( $\vec{S} = S_E \hat{x} + S_N \hat{y}$ , where  $S_E, S_N = [-3, 3]$  s/km). As an example, the best fit slowness vector for the 13 February tornillo (Figure 2a) was  $\vec{S} = -2.4\hat{x} + 1.9\hat{y}$  (s/km), equivalent to a propagation azimuth of 308° and an apparent velocity of 328 m/s (Figure 1c). This event was the largest in our catalog and had a peak-to-peak amplitude of 1.4 or 11.8 Pa when reduced to 1 km. Travel time from crater to CIS would have been  $24.5 \pm 0.5$  s.

The tornillos recorded at CIS between January and June of 2016 are readily picked using a match filter with an arbitrary master event. The similarity of the tornillos is remarkable and—because of this—the choice of a master event does not impact the number of detections. Eighty-eight events were identified in the first 6 months of 2016, of which the vast majority (~90%), occurred between January and March. Forty-three of these tornillos possessed peak-to-peak amplitudes greater than 0.2 Pa at CIS (8,342 m from the vent) and are displayed in the supporting information.

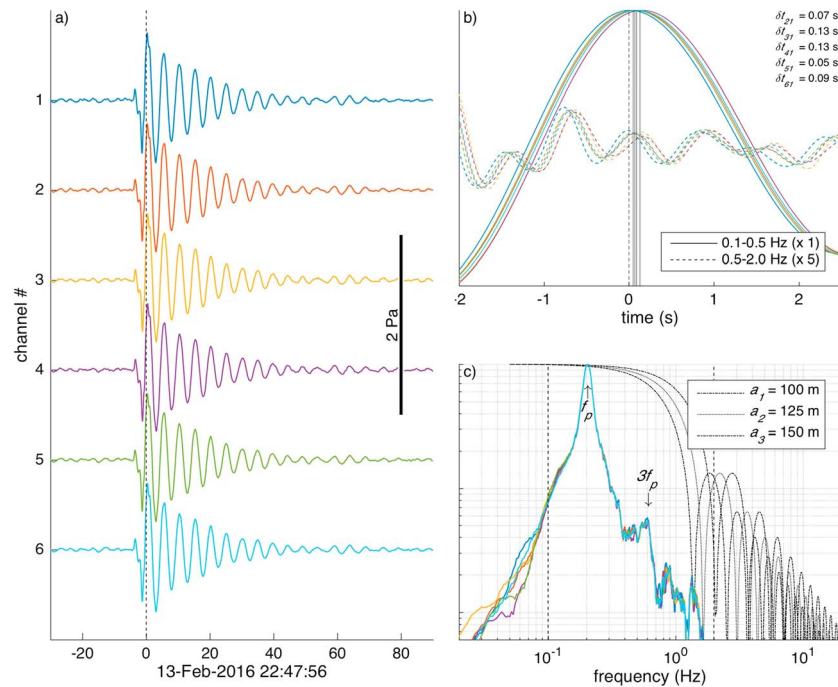


**Figure 2.** Largest tornillo recorded between January and June 2016. (a) Six-channel data recorded at the CIS array and filtered between 0.1 and 2 Hz. (b) Detail of the infrasound from panel a centered at 0 s and filtered in two different bands with relative amplification indicated. The moveout in infrasound records, indicated as phase delays relative to channel 1 ( $\delta t_{i1}$ ), corresponds to a plane wave with a normal consistent with radiation from the Cotopaxi summit (Figure 1c). (c) The log amplitude spectrum shows a dominant frequency peak at 0.2 Hz and another lower-energy peak at 3 times the fundamental frequency. Baffled piston response is shown for off-axis radiation for crater radii of 100, 125, and 150 m (black lines). These responses are calculated from Kinsler et al. (2000) (section 7.4) and suggest that the radial dimension of Cotopaxi's crater should not significantly attenuate the fundamental frequency or its first overtone at 0.6 Hz.

## 5. Tornillo Attributes

Cotopaxi infrasound tornillos are noteworthy in terms of their sustained duration as well as their stable and remarkably peaked frequency spectra. Tornillo peak frequency ( $f_p$ ) is calculated from smoothed high-resolution spectra, and the associated spectral bandwidth ( $\delta f$ ) is picked as the difference between low and high corner frequencies, that is, where power spectrum drops to one half of the power at  $f_p$ . Quality factor is then calculated as  $Q = f_p / \delta f$  and may be used to derive the exponential decay of the signal envelope where  $\alpha = \pi f_p / Q$  (Rossing & Fletcher, 2004). In general,  $Q$  is high but somewhat varied (from 7 to 17), and this may be due, at least in part, to the imprecision in picking bandwidth for smaller, lower signal-to-noise events.

Higher-mode spectral peaks of the tornillos are evident but possess diminished amplitude compared to the fundamental mode. For example, the large 13 February event (Figure 2c) has a secondary peak at 0.615 Hz corresponding to 3 times the fundamental ( $f_p = 0.205$  Hz). Odd overtones (e.g.,  $3f_p$  and  $5f_p$ ) are suggestive of “organ pipe modes” or pipes where only one end is stopped. An immense cylindrical pipe is compatible with visual observations of Cotopaxi's deep summit crater in 2016. Reduced amplitude of the odd overtones may be attributed to the noncompact size of the piston-type radiator (Figure 3c), preferential atmospheric transmission attenuation of the higher modes, and/or a source time function that is dominated by low-frequency accelerations.

The far-field infrasound pressure records may be used to estimate acoustic strength for volumetric sources. Assuming a linear acoustic source that is compact with respect to the radiated infrasound wavelengths, the cumulative volume flux is proportional to twice integrated infrasound pressure, that is,  $V(t) = 2\pi r / \rho_a \int (\int \delta p(t + r/c_a) dt) dt$  where the infrasound record is delayed by the transmission time  $r/c_a$  (e.g., Johnson & Miller, 2014). This equation implies that the responsible source volume time history at the crater outlet is also a decaying oscillation peaked at  $\sim 0.2$  Hz. Assuming a transmission distance

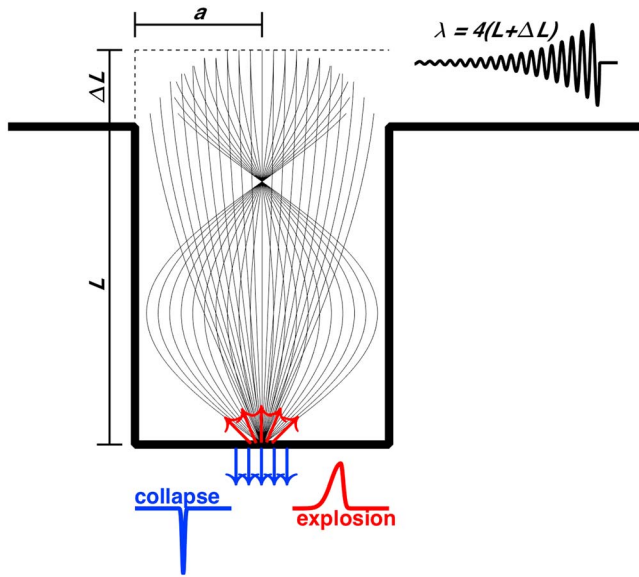


**Figure 3.** Idealized geometry of Cotopaxi's crater consisting of a vertical pipe embedded in a half space. Crater radius ( $a$ ) and length ( $L$ ) are shown with a 1:2.5 aspect ratio and  $L_{\text{eff}}$  is indicated as  $L + \Delta L$ . The fundamental wave-lengths of the resonant mode ( $4 L_{\text{eff}}$ ) and first overtone ( $4/3 L_{\text{eff}}$ ) are shown schematically as sinusoids. Schematic illustration of volume flux time series at the bottom of the crater include floor collapse (blue time series) and explosion outflux indicated by gradual onset and rapid taper (red time series). Both sources could give rise to infrasound observations possessing primarily rarefaction pressure onsets and coda with characteristic wave-lengths  $4(L + \Delta L)$ .

$r = 8342$  m and atmospheric density  $\rho_a = 0.66$  kg/m<sup>3</sup> the peak volume output is initially  $10^5$  m<sup>3</sup> for the largest tornillo occurring on 13 February. Averaged over a crater with radius  $\sim 10^2$  m, this equates to a vertical source displacement of  $\pm 1$  m.

## 6. Cotopaxi's "Organ Pipe"

We propose that a pipe many hundreds of meters in length gives rise both to the very low fundamental frequency of the infrasound tornillo and to the high quality factor of the infrasound that is sourced from the crater. We estimate the depth, or length, to the crater's bottom by modeling the crater as a straight conduit (with top end open and the bottom closed) of constant radius ( $a$ ) and uniform temperature ( $T$ ; Figure 3). In the familiar case of a very narrow pipe the sound wave-length is equivalent to 4 times the pipe length ( $L$ ). For the case where the pipe width is relatively large, and end effects must be considered, the additional length ( $\Delta L$ ) is dependent upon the pipe radius. We consider the case of a flanged pipe (Kinsler et al., 2000, section 10.2; Vidal et al., 2006), which corresponds to a vertical-walled crater shaft of length  $L$  embedded in a solid half space. The effective pipe length is then

$$L_{\text{eff}} = L + \Delta L = L + \frac{8}{3\pi}a = \frac{1}{4} \frac{c}{f_p}, \quad (1)$$

where  $c$  is sound speed in the conduit/crater.

The quality factor of a straight pipe ( $Q_r$ ) due to radiation through its outlet is a function of its aspect ratio, that is, length divided by radius. For an open-closed pipe an analytical expression for  $Q_r$  due to radiation is given as (Kinsler et al., 2000, section 10.3; Moloney & Hatten, 2001) follows:

$$Q_r = \frac{4 L L_{\text{eff}}}{\pi a a} = \frac{4 L^2}{\pi a^2} + \frac{32 L}{3\pi^2 a}. \quad (2)$$

In the case where intrinsic propagation losses due to viscous attenuation and crater wall absorption are small (i.e.,  $Q_i \rightarrow \infty$ ) the measured infrasound signal quality factor will be nearly the same as the tube's radiation quality factor (e.g., Kumagai & Chouet, 1999),

$$Q^{-1} = Q_r^{-1} + Q_i^{-1} \cong Q_r^{-1}. \quad (3)$$

Assuming that  $Q \cong Q_r$ , rearrangement of equation (2) permits an expression for the pipe length,

$$L = a \left[ \sqrt{\frac{16}{9\pi^2} + \frac{\pi}{4} Q} - \frac{4}{3\pi} \right], \quad (4)$$

and the combination of equations (1) and (4) leads to an expression for conduit sound speed:

$$c = 4 a f_p \left[ \sqrt{\frac{16}{9\pi^2} + \frac{\pi}{4} Q} + \frac{4}{3\pi} \right]. \quad (5)$$

For homogeneous conditions within the crater the gas temperature is  $T = c^2/\gamma R$ , where  $\gamma = 1.4$  for an ideal gas and  $R$  is the specific gas constant related to the molar mass of the gas species. We consider that values of  $R$  could range from  $287$  J·kg<sup>-1</sup>·K<sup>-1</sup> for dry air to lower values if substantial CO<sub>2</sub> ( $R = 189$  J·kg<sup>-1</sup>·K<sup>-1</sup>) or SO<sub>2</sub> ( $R = 130$  J·kg<sup>-1</sup>·K<sup>-1</sup>) is present. Supposing the crater is composed of 10% CO<sub>2</sub> and 10% SO<sub>2</sub>, the ideal gas constant would be  $\sim 262$  J·kg<sup>-1</sup>·K<sup>-1</sup>, some 10% less than that for dry air. In Figure 4 we consider end-member gas constant values of 287 and 262 J·kg<sup>-1</sup>·K<sup>-1</sup> to permit estimation of temperature from sound speed.

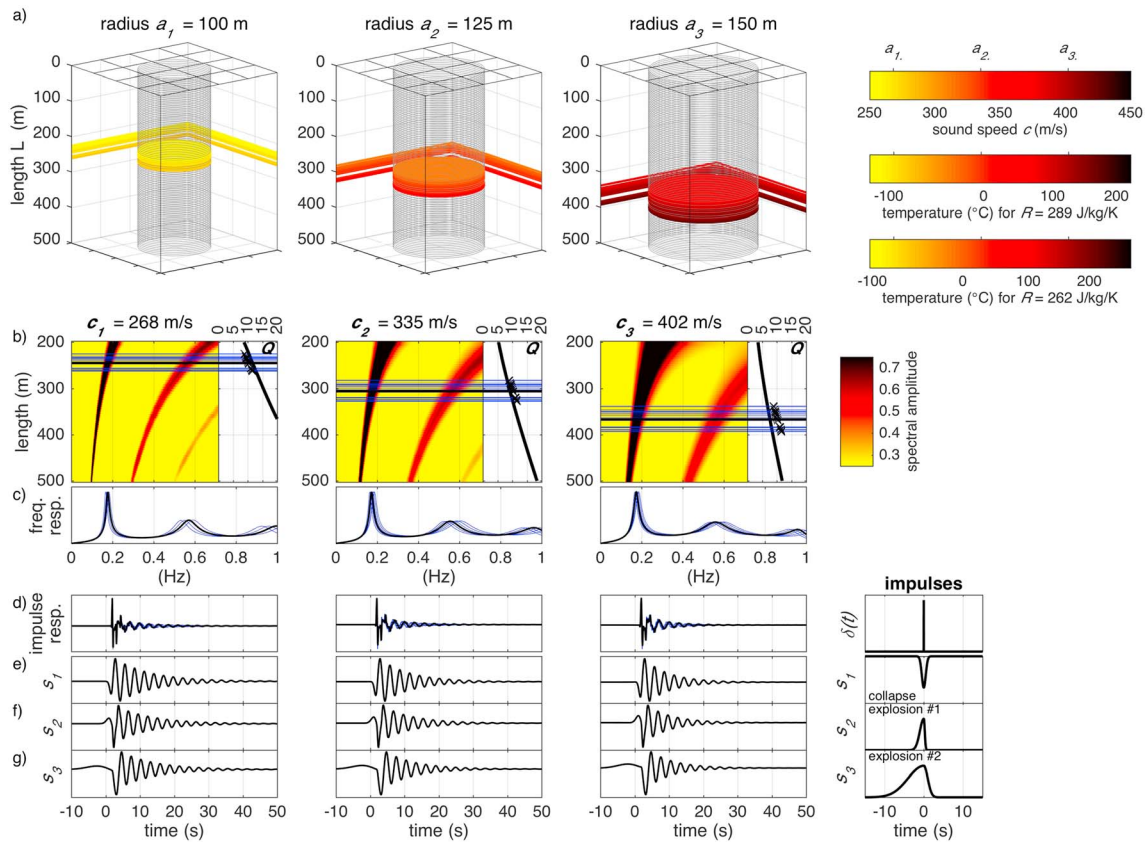


**Figure 4.** Inferred crater geometries and synthetic infrasound. Row (a) depth of crater ( $L$ ) along with color-coded sound speed ( $c$ ) and temperatures ( $T$ ) as a function of three different crater radii ( $a_1 = 100$ ,  $a_2 = 125$ , and  $a_3 = 150$  m; refer to Figures 1a and 1b). Crater parameters ( $L$  and  $c$ ) are calculated according to equations (4) and (5). Color bars show sound speed and temperatures (for two values of  $R$ ). Mean values of  $c$  and  $T$  are indicated as  $a_1$ ,  $a_2$ , and  $a_3$ . Row (b) amplitude spectra for crater geometry and specified sound speed shown as a function of crater length and prescribed radius. Horizontal lines denote the crater lengths indicated in row (a).  $Q$  is provided as a function of depth for the numerical solutions (black line) and for the analytical solutions (x symbols; equation (4)). Row (c) amplitude spectra for spectrum of depths (blue lines in b) and for the mean solution (black line in b). Row (d) corresponding impulse responses calculated according to 1-D modeling following the method described in Johnson et al. (2018). The impulse responses are convolved with row (e) a negative Gaussian pulse, row (f) an asymmetric Gaussian source-time function, and row (g) a long-period asymmetric Gaussian. The respective source-time functions are shown in the rightmost column for rows (d)–(g).

We use  $f_p$  and  $Q$  to estimate both conduit length and temperatures for crater radii ranging from 100 to 150 m, dimensions which conservatively encompass end-member radius estimates from aerial overflight observations (Figures 1a and 1b). From our distribution of  $Q$  values for tornillo signals the interquartile range spans 8.77 to 11.96 for 22 events (supporting information). Using these  $Q$  values, inferred crater depth and temperatures cluster for a specified conduit radius (Figure 4a). For example, a crater radius of 125 m corresponds to conduit depths/lengths of  $306 \text{ m} \pm 7\%$  and an average sound speed of  $335 \text{ m/s} \pm 6\%$ . The mean sound speed of 335 m/s is attributable to temperatures ranging from 4 to  $32^\circ\text{C}$  depending upon the choice of gas composition. A wider crater radius of 150 m yields depth/length values of 367 m with an average sound speed of 402 m/s ( $126$  to  $167^\circ\text{C}$  depending upon  $R$ ). This wider crater dimension is larger than the photogrammetric observations and its inferred temperatures are higher than those seen in thermal imagery for the crater wall. A narrower conduit of 100 m gives rise to what we consider unreasonably low ( $\sim -80^\circ\text{C}$ ) temperatures.

Modeling indicated in Figure 4 suggests that Cotopaxi crater is around 125 m in radius and has a conduit length between about 270 and 320 m. These vertical dimensions are substantial and are supported by sporadic aerial observations where the floor of the crater is considered “very deep” because it is out of view. These crater lengths are also greater than the crater dimensions inferred from resonant volcano infrasound reported at other volcanic systems, where the infrasound tends to be of higher frequency. For example, resonant frequencies at Pagan and at Kilauea are on the order of 0.3 Hz and have been attributed to a funnel-



shaped and vertical-walled ~200-m-deep craters, respectively (Fee et al., 2010; Lyons et al., 2016). Resonant infrasound from the various craters at Etna exhibit a variety of fundamental frequencies, often around 1 Hz, but with some craters produce tones as low as 0.25 Hz, and these are attributed to a range of conduit lengths above the magma free surface (Spina et al., 2014). At Villarrica, resonant frequencies between 0.5 and 1.2 Hz have been attributed to dynamically varying crater lengths on the order of 50–200 m (Johnson et al., 2018; Richardson et al., 2014).

In many of the previous studies at other volcanic systems the frequency content of the resonant infrasound is time variable (Fee et al., 2010; Johnson et al., 2018; Richardson et al., 2014; Spina et al., 2014), but the observed Cotopaxi tornillos are relatively stable over the period of observation. Cotopaxi's modeled crater length variations on the order of  $\pm 25$  m may be attributable to noise in the derived data parameters ( $Q$  and  $f_p$ ) and/or failure to adequately consider possible influence of intrinsic attenuation due to wall absorption (i.e.,  $Q_i^{-1}$ ). Alternatively, variations in inferred depth could be attributed to time-varying changes in the system including the conduit depth, conduit radius, temperature within the conduit, or gas composition in the conduit. We cannot rule these variables out, but we consider that substantial morphological fluctuations are relative unlikely because we observe no systematic changes in  $Q$  and  $f_p$  over time. Although craters, or conduits, may conceivably widen over time, they are not likely to constrict (e.g., Ortiz et al., 2018). Similarly, though crater floors may progressively drop as a system depressurizes at the conclusion of an eruptive period, crater floor ascent, or oscillations of the depth to a crater floor, is less likely given the absence of conjoint geodetic or seismic signal.

## 7. On the Potential Source Mechanism for the Cotopaxi Tornillo

The excitation of acoustic tornillo-like waveforms has been demonstrated in small-scale laboratory experiments where  $10^{-1}$ -m length pipes are pressurized until a soap bubble membrane is ruptured at the pipe's outlet (Vidal et al., 2006). The pipe then becomes an open-closed resonator sustaining oscillations whose quality factor is determined by the tube aspect ratio. Although these experiments yield signals with some 5,000-fold-higher acoustic frequencies than the 0.2-Hz Cotopaxi tornillos, the resultant time series from lab experiments are remarkably similar in terms of signal envelope suggesting scalability of analog experiments. It is notable that the acoustic tornillos can be excited by short duration source impulses.

In laboratory experiments the microphones placed outside the pipe record compressional first motions or an initial increase in excess pressure after membrane rupture (Vidal et al., 2006). Compressional first arrivals are also observed for analog experiments where "explosions" are simulated near the bottom of a pipe (Sanchez et al., 2014). Cotopaxi's infrasound tornillos, on the other hand, seem to exhibit predominantly dilatational, ambiguous, or emergent first motions (e.g., Figure 2; supporting information). The observation of a negative initial pressure pulse is notable and suggestive of either an implosive initial motion at the base of the conduit or a significantly phase-shifted first arrival.

We first consider that a rarefactory first motion might potentially result from sudden downward collapse of the crater floor (Figures 3 and 4e). Such collapse could be due to magma or hydrothermal fluid withdrawal albeit with a net motion smaller than the well-documented large crater floor collapses at Miyakejima (Japan; Geshi et al., 2002) or Piton de la Fournaise (Réunion; Staudacher et al., 2009), which both had significant seismic response. Supposing that magma drawdown or gas venting during 2016 left small voids beneath Cotopaxi's crater, it might be reasonable that piecemeal collapse of the crater floor over weeks to months could give rise to repeated rarefactory infrasound transients.

An alternative explanation for Cotopaxi's apparent negative infrasound polarity might be the substantial modulating influence of the Cotopaxi crater itself. Generally, a discrete explosive source occurring without obstruction at the top of a volcano results in a characteristic bipolar infrasound signal composed of an initial compression followed by a rarefaction (e.g., Johnson et al., 2004; Marchetti et al., 2013); however, given the extreme crater response associated with a long narrow cylinder, a volumetric source-time function may be substantially filtered.

Cotopaxi crater's acoustic response can be calculated numerically for prescribed 1-D radial symmetry following the model outlined in Johnson et al. (2018). Synthetics shown in Figure 4 correspond to the transfer function between a volume flux source  $s(t)$  distributed across the floor of a flat crater and the pressure records

radiated to the far field. The modeling includes the effects of off-axis sound radiation for an assumed baffled piston at the crater's outlet. The model permits derivation of both frequency and impulse responses (Figures 4c and 4d) for the crater geometries calculated from equation (4) (Figure 4a). Quality factors derived from these synthetic spectra compare favorably with the data's  $Q$ ; however, the differences between numerical and analytical  $Q$  are slightly more significant for wider craters. We suppose this is due to the modeling assumption that  $ka \ll 1$  (where wave number  $k = 2\pi/\lambda \cong 0.003 \text{ m}^{-1}$  for  $\sim 0.2$ -Hz infrasound).

The impulse response can be used to synthesize infrasound pressure records for arbitrary source-time functions. To simulate negative initial polarity, we consider candidate source time functions including an implosive or collapsing source (Figure 4e) and two types of explosions with asymmetric acoustic flow histories and relatively short (Figure 4f) and long (Figure 4g) durations. Such time histories may be thought of as explosions, or gas emissions, which start relatively nonimpulsively. The two examples given in Figures 4f and 4g, with rise times of 2.5 and 10 s, are convolved with crater impulse responses to demonstrate that initial polarity may become either ambiguous or diminished in size. We consider that variations in the duration of explosive degassing may provide a reasonable explanation for the substantial variability in the onset characteristics of recorded tornillos (see supporting information). Coincident webcam observations of ash and vapor emissions further supports the hypothesis that Cotopaxi tornillos are related to explosion events.

## 8. Conclusions

Volcano infrasound is produced by a variety of sources occurring at the atmosphere/solid Earth interface in response to dynamic processes. Recorded infrasound, often acquired many kilometers from a volcano source, represents a modified source time function that is modulated by intervening atmosphere and topography, including at both the source and receiver. The Cotopaxi tornillos represent a particularly significant modulation of what might be relatively simple sources, possibly explosions occurring at the bottom of the crater. The deep, steep-walled summit crater of Cotopaxi exerts a particularly strong filter giving rise to both high- $Q$  oscillations and apparent rarefactory signal onsets. More generally, these findings suggest that the influence of crater response functions should be considered whenever volcano infrasound is analyzed.

### Acknowledgments

This work was funded in part by National Science Foundation grant EAR-0838562 and by the Geological Sciences Martin Fund at the University of North Carolina, Chapel Hill. The Instituto Geográfico Militar (IGM) from Ecuador provided the orthophoto from 28 January 2016. Japan International Cooperation Agency (JICA) network infrasound data were used in part of this study. The infrasound signals from CIS analyzed in this study are available as a permanent DOI archive at [https://scholarworks.boisestate.edu/infrasound\\_data/2/](https://scholarworks.boisestate.edu/infrasound_data/2/) and are openly shared via ScholarWorks, Boise State's institutional research repository managed by Albertsons Library and released under a creative commons license.

### References

- Bernard, B., Battaglia, J., Proaño, A., Hidalgo, S., Vásquez, F., Hernandez, S., & Ruiz, M. (2016). Relationship between volcanic ash fallouts and seismic tremor: Quantitative assessment of the 2015 eruptive period at Cotopaxi volcano, Ecuador. *Bulletin of Volcanology*, *78*(11), 1–11. <https://doi.org/10.1007/s00445-016-1077-5>
- De Angelis, S. (2006). Analyses of unusual long-period earthquakes with extended coda recorded at Katmai National Park, Alaska, USA. *Geophysical Research Letters*, *33*, L07306. <https://doi.org/10.1029/2005GL025581>
- Fee, D., Garcés, M., Patrick, M., Chouet, B., Dawson, P., & Swanson, D. (2010). Infrasonic harmonic tremor and degassing bursts from Halema'uma'u Crater, Kilauea Volcano, Hawaii. *Journal of Geophysical Research*, *115*, B11316. <https://doi.org/10.1029/2010JB007642>
- Gaunt, H. E., Bernard, B., Hidalgo, S., Proaño, A., Wright, H., Mothes, P., et al. (2016). Juvenile magma recognition and eruptive dynamics inferred from the analysis of ash time series: The 2015 reawakening of Cotopaxi volcano. *Journal of Volcanology and Geothermal Research*, *328*, 134–146. <https://doi.org/10.1016/j.jvolgeores.2016.10.013>
- Geshi, N., Shimano, T., Chiba, T., & Nakada, S. (2002). Caldera collapse during the 2000 eruption of Miyakejima Volcano, Japan. *Bulletin of Volcanology*, *64*(1), 55–68. <https://doi.org/10.1007/s00445-001-0184-z>
- Gómez, M. D. M., & Torres, C. R. A. (1997). Unusual low-frequency volcanic seismic events with slowly decaying coda waves observed at Galeras and other volcanoes. *Journal of Volcanology and Geothermal Research*, *77*(1–4), 173–193. [https://doi.org/10.1016/S0377-0273\(96\)00093-5](https://doi.org/10.1016/S0377-0273(96)00093-5)
- Goto, A., & Johnson, J. B. (2011). Monotonic infrasound and Helmholtz resonance at Volcan Villarrica (Chile). *Geophysical Research Letters*, *38*, L06301. <https://doi.org/10.1029/2011GL046858>
- Hagerty, M., & Benites, R. (2003). Tornillos beneath Tongariro Volcano, New Zealand. *Journal of Volcanology and Geothermal Research*, *125*(1–2), 151–169. [https://doi.org/10.1016/S0377-0273\(03\)00094-5](https://doi.org/10.1016/S0377-0273(03)00094-5)
- Johnson, J. B., Aster, R. C., & Kyle, P. R. (2004). Volcanic eruptions observed with infrasound. *Geophysical Research Letters*, *31*, 21–24. <https://doi.org/10.1029/2004GL020020>
- Johnson, J. B., & Miller, A. J. C. (2014). Application of the monopole source to quantify explosive flux during Vulcanian explosions at Sakurajima Volcano (Japan). *Seismological Research Letters*, *85*(6), 1163–1176. <https://doi.org/10.1785/0220140058>
- Johnson, J. B., Watson, L. M., Palma, J. L., Dunham, E. M., & Anderson, J. F. (2018). Forecasting the eruption of an open-vent volcano using resonant infrasound tones. *Geophysical Research Letters*, *45*, 2213–2220. <https://doi.org/10.1002/2017GL076506>
- Kinsler, L. E., Frey, A. R., Coppens, A. B., & Sanders, J. V. (2000). *Fundamentals of acoustics* (4th ed.). New York: John Wiley.
- Konstantinou, K. I. (2015). Tornillos modeled as self-oscillations of fluid filling a cavity: Application to the 1992–1993 activity at Galeras volcano, Colombia. *Physics of the Earth and Planetary Interiors*, *238*, 23–33. <https://doi.org/10.1016/j.pepi.2014.10.014>
- Kumagai, H., & Chouet, B. A. (1999). The complex frequencies of long-period seismic events as probes of fluid composition beneath volcanoes. *Geophysical Journal International*, *138*(2), F7–F12. <https://doi.org/10.1046/j.1365-246X.1999.00911.x>
- Lesage, P., & Suroño, P. (1995). Seismic precursors of the February 10, 1990 eruption of Kelut volcano, Java. *Journal of Volcanology and Geothermal Research*, *65*(1–2), 135–146. [https://doi.org/10.1016/0377-0273\(94\)00051-H](https://doi.org/10.1016/0377-0273(94)00051-H)

- Lyons, J. J., Haney, M. M., Werner, C., Kelly, P., Patrick, M., Kern, C., & Trusdell, F. (2016). Long period seismicity and very long period infrasound driven by shallow magmatic degassing at Mount Pagan, Mariana Islands. *Journal of Geophysical Research: Solid Earth*, *121*, 188–209. <https://doi.org/10.1002/2015JB012490>
- Marchetti, E., Ripepe, M., Delle Donne, D., Genco, R., Finizola, A., & Garaebiti, E. (2013). Blast waves from violent explosive activity at Yasur Volcano, Vanuatu. *Geophysical Research Letters*, *40*, 5838–5843. <https://doi.org/10.1002/2013GL057900>
- Marcillo, O., Johnson, J. B., & Hart, D. (2012). Implementation, characterization, and evaluation of an inexpensive low-power low-noise infrasound sensor based on a micro-machined differential pressure transducer and a mechanical filter. *Journal of Atmospheric and Oceanic Technology*, *29*(9), 1275–1284. <https://doi.org/10.1175/JTECH-D-11-00101.1>
- Moloney, M. J., & Hatten, D. L. (2001). Acoustic quality factor and energy losses in cylindrical pipes. *American Journal of Physics*, *69*(3), 311–314. <https://doi.org/10.1119/1.1308264>
- Narváez, M. L., Torres, C. R. A., Gómez, M. D. M., Cortés, J. G. P., Cepeda, V. H., & Stix, J. (1997). “Tornillo”-type seismic signals at Galeras volcano, Colombia, 1992–1993. *Journal of Volcanology and Geothermal Research*, *77*(1–4), 159–171. [https://doi.org/10.1016/S0377-0273\(96\)00092-3](https://doi.org/10.1016/S0377-0273(96)00092-3)
- Ortiz, H. D., Johnson, J. B., Ramón, P. G., & Ruiz, M. C. (2018). Using infrasound waves to monitor tropospheric weather and crater morphology changes at Volcán Tungurahua, Ecuador. *Journal of Volcanology and Geothermal Research*, *349*, 205–216. <https://doi.org/10.1016/j.jvolgeores.2017.11.001>
- Richardson, J. P., Waite, G. P., & Palma, J. L. (2014). Varying seismic-acoustic properties of the fluctuating lava lake at Villarrica volcano, Chile. *Journal of Geophysical Research: Solid Earth*, *119*, 5560–5573. <https://doi.org/10.1002/2014JB011002>
- Rossing, T. D., & Fletcher, N. H. (2004). *Principles of vibration and sound* (2nd ed., pp. 157–207). New York: Springer.
- Rowe, C. A., Aster, R. C., Kyle, P. R., Dibble, R. R., & Schlue, J. W. (2000). Seismic and acoustic observations at Mount Erebus Volcano, Ross Island, Antarctica, 1994–1998. *Journal of Volcanology and Geothermal Research*, *101*(1–2), 105–128. [https://doi.org/10.1016/S0377-0273\(00\)00170-0](https://doi.org/10.1016/S0377-0273(00)00170-0)
- Sanchez, C., Alvarez, B., Melo, F., & Vidal, V. (2014). Experimental modeling of infrasound emission. *Geophysical Research Letters*, *41*, 6705–6711. <https://doi.org/10.1002/2014GL061068>
- Shimozuru, D., & Kagiya, T. (1989). Some significant features of pre-eruption volcanic earthquakes. In J. H. Latter (Ed.), *Volcanic hazards. IAVCEI Proceedings in volcanology* (Vol. 1, pp. 504–512). Berlin: Springer. [https://doi.org/10.1007/978-3-642-73759-6\\_28](https://doi.org/10.1007/978-3-642-73759-6_28)
- Spina, L., Cannata, A., Privitera, E., Vergnolle, S., Ferlito, C., Gresta, S., et al. (2014). Insights into Mt. Etna’s shallow plumbing system from the analysis of infrasound signals, August 2007–December 2009. *Pure and Applied Geophysics*, *172*(2), 473–490. <https://doi.org/10.1007/s00024-014-0884-x>
- Staudacher, T., Ferrazzini, V., Peltier, A., Kowalski, P., Boissier, P., Catherine, P., et al. (2009). The April 2007 eruption and the Dolomieu crater collapse, two major events at Piton de la Fournaise (La Réunion Island, Indian Ocean). *Journal of Volcanology and Geothermal Research*, *184*(1–2), 126–137. <https://doi.org/10.1016/j.jvolgeores.2008.11.005>
- Troncoso, L., Bustillos, J., Romero, J. E., Guevara, A., Carrillo, J., Montalvo, E., & Izquierdo, T. (2017). Hydrovolcanic ash emission between August 14 and 24, 2015 at Cotopaxi volcano (Ecuador): Characterization and eruption mechanisms. *Journal of Volcanology and Geothermal Research*, *341*, 228–241. <https://doi.org/10.1016/j.jvolgeores.2017.05.032>
- Vidal, V., Géminard, J. C., Divoux, T., & Melo, F. (2006). Acoustic signal associated with the bursting of a soap film which initially closes an overpressurized cavity: Experiment and theory. *European Physical Journal B*, *54*(3), 321–339. <https://doi.org/10.1140/epjb/e2006-00450-0>